The Astrophysical Journal, 835:214 (12pp), 2017 February 1 doi:10.3847/1538-4357/835/2/214

Stochastic Fermi Energization of Coronal Plasma during Explosive Magnetic Energy Release

Theophilos Pisokas[1], Loukas Vlahos[1], Heinz Isliker[1], Vassilis Tsiolis[1], and Anastasios Anastasiadis[2]
[1] Department of Physics, Aristotle University of Thessaloniki GR-52124 Thessaloniki, Greece
[2] Institute for Astronomy, Astrophysics, Space Applications and Remote Sensing, National Observatory of Athens GR-15236 Penteli, Greece
Received 2016 September 7; revised 2016 November 20; accepted 2016 December 10; published 2017 January 31

Abstract

The aim of this study is to analyze the interaction of charged particles (ions and electrons) with randomly formed particle scatterers (e.g., large-scale local "magnetic fluctuations" or "coherent magnetic irregularities") using the setup proposed initially by Fermi. These scatterers are formed by the explosive magnetic energy release and propagate with the Alfvén speed along the irregular magnetic fields. They are large-scale local fluctuations ($\delta B/B \approx 1$) randomly distributed inside the unstable magnetic topology and will here be called Alfvénic Scatterers (AS). We constructed a 3D grid on which a small fraction of randomly chosen grid points are acting as AS. In particular, we study how a large number of test particles evolves inside a collection of AS, analyzing the evolution of their energy distribution and their escape-time distribution. We use a well-established method to estimate the transport coefficients directly from the trajectories of the particles. Using the estimated transport coefficients and solving the Fokker–Planck equation numerically, we can recover the energy distribution of the particles. We have shown that the stochastic Fermi energization of mildly relativistic and relativistic plasma can heat and accelerate the tail of the ambient particle distribution as predicted by Parker & Tidman and Ramaty. The temperature of the hot plasma and the tail of the energetic particles depend on the mean free path (λ_{sc}) of the particles between the scatterers inside the energization volume.

Key words: acceleration of particles – Sun: corona – Sun: coronal mass ejections (CMEs) – Sun: flares – turbulence

1. Introduction

The stochastic acceleration was first proposed and analyzed by Fermi (1949) as a mechanism for the acceleration of cosmic rays (Longair 2011, see details and references therein). The core of his idea, which we call here stochastic Fermi energization (SFE), had a larger impact on nonlinear processes in general and has been the driving force behind all subsequent theories on charged particle energization in space and astrophysical plasmas. In the original treatment, relativistic particles were accelerated by encounters with very massive, slowly moving magnetic clouds (scattering centers). Fermi also dropped (without any justification) the stochastic energy change and kept only the systematic rate of energy gain, focusing on the interaction of scatterers with the high-energy tail of protons. The rate of the systematic energy gain of the charged particles with the scatterers is proportional to the square of the ratio of the magnetic cloud speed (V) to the speed of light (c), i.e., $(V/c)^2$. A few years after the initial paper by Fermi, Davis (1956) and Parker & Tidman (1958) emphasized the stochastic nature of the initial Fermi proposal and they analytically estimated the transport coefficients using an idealized assumption for the interaction of the scatterers with the particles. Parker & Tidman (1958) and Ramaty (1979) assumed that the scattering centers are randomly moving hard spheres and applied their model to solar flares for accelerating protons from the thermal distribution.

The initial idea put forward by Fermi was soon replaced in astrophysical literature with a new suggestion based on the interaction of charged particles with a Kolmogorov spectrum of low amplitude MHD waves ($\delta B/B \ll 1$) and the acceleration process was renamed as stochastic (weak) turbulent heating and acceleration or simply stochastic acceleration by turbulence (SAT; see Davis 1956; Tverskoi 1967; Kulsrud & Ferrari 1971; see also the reviews by Miller et al. 1997; Petrosian 2012). When the amplitude of the waves (δB) is much smaller than the mean magnetic field B, the transport coefficients for the SAT are estimated with the use of the quasilinear approximation; by solving the transport equations one can estimate the evolution of the energy distribution of the particles (see Achterberg 1981; Schlickeiser 1989). So, the SFE was replaced in the recent years by SAT and the Fokker–Planck (FP) equation became the main tool for the analysis of the evolution of energy distributions of particles.

In the solar atmosphere, the formation of scatterers from traveling large-scale Alfvén wave packets, deformed by irregular magnetic fields inside a complex magnetic topology and driven by the turbulent convection zone and/or the photospheric motions, has been analyzed by Similon & Sudan (1989). They showed that complicated magnetic geometry, typical to most astrophysical plasmas, greatly reduces the dissipation length, as compared to laminar fields. Parker (1994) pointed out that the spontaneous formation of magnetic discontinuities inside a driven complex magnetic topology can cause explosive events (nanoflares, microflares, flares, and coronal mass ejections (CME)), which can become the source of torsional Alfvén waves propagating along the mean magnetic field, developing increasingly complex structures when they propagate along the stochastic magnetic field lines. Hence, the onset of flares of all scales arises in the strongly interwoven flux bundles and drives Alfvén wave packets (Parker 1983). Fletcher & Hudson (2008) suggested that the energy stored in preflare coronal magnetic field can be rapidly converted and liberated by coronal magnetic field reconfiguration and relaxation during flares. The sudden reconfiguration will generate large-scale wave pulses, which transport energy

rapidly through the corona and the lower atmosphere. Their analysis was restricted to laminar magnetic fields and simple magnetic loops and excluded the formation of Alfvén Scatterers (AS) and unstable current sheets (UCS), which are expected if the large-scale MHD waves propagate along complex field lines.

The majority of the 3D MHD simulations of explosive solar energy release start with a simple magnetic topology that is forced away from equilibrium. During the eruption or shortly after, the magnetic field becomes complex and liberates large-scale magnetic disturbances due to its rapid reconfiguration. The literature on this topic is vast, since the avenues for the explosive events are several, e.g., stochastic shuffling (braiding) of the magnetic fields at the footpoints of loops (Galsgaard & Nordlund 1996), magnetic flux emergence (Archontis 2008; Schmieder et al. 2014), and the loss of stability of coronal loops (Gerrard & Hood 2003; Gordovskyy & Browning 2011, 2012; Amari et al. 2013; Leake et al. 2014; Török et al. 2014; Fletcher et al. 2015). The important points to stress here are as follows. (1) The explosive solar events are associated with complex magnetic topologies; (2) the reconfiguration of the large-scale magnetic topology, due to reconnection, will drive large-scale MHD disturbances propagating inside the 3D unstable structure; (3) the entire unstable magnetic topology will form AS and UCS, which participate in the heating and acceleration of the solar plasma trapped by this structure, as we will show in this paper.

We pose three fundamental questions. (1) Is the SAT a good approximation for the SFE? (2) Is the simple expression for the escape time, $t_{\rm esc} = L/v$ (where L is the characteristic size of the acceleration volume and v is the characteristic velocity of the accelerated particles), used extensively in the current literature, a valid approximation for the SFE? (3) How do trapped particles (in closed or open simulation boxes) evolve during the SFE?

In this study, we assume that coherent magnetic structures traveling with the Alfvén speed (Alfvénic Scatterers) can be formed by the interaction of the large-amplitude magnetic fluctuations propagating along the complex magnetic topology inside the solar atmosphere. Their excitation can be either through the motion of the plasma inside the convection zone and/or the photosphere, by emerging flux, or by sudden energy release during large-scale magnetic reconnection in the solar corona. We concentrate in this paper on the interaction of the plasma with AS. The interaction of electrons and ions with UCS was discussed briefly by Vlahos et al. (2016).

The outline of the present work is as follows. In the next section, we recapitulate the main assumptions of the stochastic Fermi type mechanism for particle acceleration and heating, and compare the main results with the stochastic weakly turbulent acceleration. In Section 3, we construct a model based on a 3D lattice approach, where scatterers can easily be replaced by different types of local accelerators, and we apply this model to the solar corona where the "scatterers" are local fluctuations, called here AS. The simulation box is assumed to be open or with periodic boundary conditions and the role of collisions is explored. In Section 4, we discuss the importance of our results in the context of the heating and acceleration of particles in the solar corona, and in Section 5 we summarize the main results of our study.

2. The Critical Assumptions of the SFE and its Relation with SAT

Fermi (1949) based the proposed acceleration mechanism and his estimates on several assumptions. Let us briefly discuss these assumptions, since some of them are not obvious in the current literature (see Longair 2011).

(1) The particles move with relativistic velocity u and the scatterers ("magnetic clouds") move with mean speed V, much smaller than the speed of light.

(2) The energy gain or loss of the particles interacting with the scatterers is

$$\frac{\Delta W}{W} \approx \frac{2}{c^2}(V^2 - \boldsymbol{V}\cdot\boldsymbol{v}), \tag{1}$$

where $\boldsymbol{V}\cdot\boldsymbol{v} < 0$ for head-on collisions where the particles gain energy, and $\boldsymbol{V}\cdot\boldsymbol{v} > 0$ for overtaking collisions where the particles lose energy ($\boldsymbol{v} = \boldsymbol{u}/\gamma$, with γ the Lorenz factor).

(3) The rate of energy gain is estimated from the relation

$$\frac{dW}{dt} = \frac{W}{t_{\rm acc}} = aW, \tag{2}$$

where

$$a = \frac{1}{t_{\rm acc}} = \frac{4}{3}\left(\frac{V}{c}\right)^2\left(\frac{c}{\lambda_{\rm sc}}\right) \tag{3}$$

and $\lambda_{\rm sc}$ is the mean free path the particles travel between the scatterers.

(4) Assuming that the distribution of the scatterers is uniform inside the acceleration volume with density $n_{\rm sc}$, the mean free path will be $\lambda_{\rm sc} \approx \frac{1}{\sqrt[3]{n_{\rm sc}}}$. The assumption that the scatters are uniformly distributed in space is a strong assumption in turbulent systems. Turbulent systems tend to be highly anisotropic and so also the distribution of the scatterers may not be isotropic.

(5) The particles are not trapped inside the scatterers, their interaction is instantaneous.

(6) Solving Equation (2), we can estimate the temporal evolution of the mean energy as

$$\langle W(t)\rangle = W_0 e^{at}. \tag{4}$$

(7) Fermi (1949) used the diffusion (FP) equation in order to estimate the evolution of the energy distribution $n(W, t)$ of the accelerated particles. In order to simplify the diffusion equation, he assumed that spatial diffusion is not important and the particles diffuse only in energy space,

$$\frac{\partial n}{\partial t} + \frac{\partial}{\partial W}\left[Fn - \frac{\partial (Dn)}{\partial W}\right] = -\frac{n}{t_{\rm esc}} + Q, \tag{5}$$

where $t_{\rm esc}$ is the escape time from an acceleration volume with characteristic length L, injection rate Q, and transport coefficients F and D.

Fermi reached his famous result by assuming that (a) the energy distribution reached an asymptotic state before the particles escaped from the acceleration volume and (b) the energy diffusion coefficient approaches zero ($D \sim 0$) asymptotically for relativistic particles and the acceleration is mainly due to the systematic acceleration, which, according to

Equation (2), is given as

$$F(W, t) = \left\langle \frac{dW}{dt} \right\rangle_W = aW. \quad (6)$$

Based on all of the assumptions mentioned above, the asymptotic solution of Equation (5) is simply

$$n(W) \sim W^{-k}, \quad (7)$$

where

$$k = 1 + \frac{t_{\rm acc}}{t_{\rm esc}}. \quad (8)$$

The index k approaches 2, which is close to the observed value for the cosmic-ray spectrum, only if $t_{\rm acc} \approx t_{\rm esc}$, $at_{\rm esc} \sim 1$. In most recent theoretical studies of the stochastic Fermi acceleration, the escape time (which is so crucial for the estimate of k) is difficult to estimate quantitatively (Miller et al. 1990; Petrosian 2012).

Parker & Tidman (1958) and Ramaty (1979) analyzed the interaction of electrons and ions with large-amplitude magnetic perturbations, which they assumed to be hard spheres in order to obtain analytical results. They estimated the transport coefficients analytically as

$$F(W) = \frac{4}{3}\alpha c \left[\frac{2W}{m}\right]^{1/2} \sim W^{0.5} \quad (9)$$

and

$$D(W) = \frac{1}{3}\alpha c [2W]^{3/2} m^{1/2} \sim W^{1.5}, \quad (10)$$

with $\alpha = (3/4)a$. The mean energy increase in the hard sphere approximation is

$$\langle W(t) \rangle \sim t^2. \quad (11)$$

The energy distribution is obtained as an analytical solution of the Fokker–Planck equation and for low-energy particles ($W \ll mc^2$) it can be approximated with the function

$$f(W) \sim K_2\left(2\sqrt{\frac{3p}{mc\ \alpha t_{\rm esc}}}\right), \quad (12)$$

where K_2 is the Bessel function of the second kind and p is the momentum of the particles. For relativistic particles ($W \gg mc^2$), the solution is

$$f(W) \sim W^{1/2-(1/2)(9+12/(\alpha\ t_{\rm esc}))^{1/2}}. \quad (13)$$

Therefore, the results reported by Fermi in his original paper should be modified for non-relativistic or relativistic particles when the analysis is based on the assumption of hard spheres. Equations (13), (7), and (8) yield the same result for $a\ t_{\rm esc} \sim 1$.

Let us now summarize the main results from the interaction of a spectrum of isotropic Alfvén waves with the ambient ions. If we assume that the spectral density W_k (energy density per unit wavenumber) is proportional to k^{-2}, we can estimate the acceleration time (see Miller et al. 1990) as

$$\frac{1}{t_{\rm acc}} \approx \left(\frac{3\pi}{64}\right)\left(\frac{V_A}{c}\right)^2\left(\frac{U_A}{U_B}\right)(c\ k_{\rm min}), \quad (14)$$

where V_A is the Alfvén speed, $k_{\rm min}$ is the minimum wavenumber, U_A is the total energy density in the Alfvén waves (obtained by integrating W_k from $k_{\rm min}$ to infinity), and U_B the energy density of the ambient magnetic field. For typical coronal parameters the ambient magnetic field is 100 G, for weak turbulence $(U_A/U_B) \approx 10^{-2}$, and with $k_{\rm min} \approx 3 \cdot 10^{-6}\,{\rm cm}^{-1}$ for the Alfvén waves to be in resonance with ions with energy as high as 10 GeV, we estimate $t_{\rm acc} \approx 15$ s and, assuming that the waves act as Fermi scatterers (see Equation (3)), their $\lambda_{\rm sc} \approx 2 \cdot 10^8$ cm. Therefore, stochastic weak Alfvénic turbulence, if everything is fine-tuned, can provide $t_{\rm acc}$ and $\lambda_{\rm sc}$ of the ions during solar flares, but it fails to provide information on the energy distribution since the escape time is qualitatively defined through a simple ballistic relation $t_{\rm esc} \approx L/v$, where L is the length of the acceleration volume.

Hamilton & Petrosian (1992) analyzed the resonant interaction of a very weak spectrum of whistler waves with electrons in the presence of collisions for trapped ($t_{\rm esc} \longrightarrow \infty$) and non-trapped electrons by using and solving the Fokker–Planck equation. They found that, for energies $E < E_c$ the particles are influenced by collisions and form a quasithermal distribution, whereas above E_c the distributions of the energetic particles are power laws. The energy E_c depends on the conditions of the ambient plasma. They have also shown that even for trapped particles ($t_{\rm esc} \longrightarrow \infty$) the interaction of the electrons with the waves reaches an asymptotic state, which is similar to the one obtained from the "leaky" acceleration volumes.

Greco et al. (2010) attempted a numerical study of Fermi acceleration by using a 2D model where ions can experience Fermi-like acceleration processes by interacting with a synthetic oscillating electromagnetic wave, which is carefully tailored to mimic magnetic fluctuations (magnetic clouds) randomly positioned within the xy-plane. The free parameter of their system is the mean free path between the "magnetic clouds," $\lambda_{\rm sc}$. Their results show an efficient heating of the ambient ions, especially when the magnetic clouds are densely packed and $\lambda_{\rm sc}$ is small. In their analysis no attempt was made to estimate the transport coefficients or to provide any comparison with the basic characteristics of the stochastic Fermi acceleration for the high-energy part of their distribution (e.g., power-law index of the accelerated particles, acceleration time, evolution of the mean energy, etc.).

A key element in our understanding of stochastic Fermi acceleration is the careful estimation of the transport coefficients and the detailed analysis of the escape time for non-trapped particles. We have therefore made an attempt to calculate both in detail in this paper. The energy diffusion coefficient can be estimated directly from the dynamics of the particles through the relation

$$D(W, t) = \frac{\langle (W(t + \Delta t) - W(t)^2 \rangle_W}{2\Delta t}, \quad (15)$$

and the energy convection coefficient, representing the systematic acceleration, is given as

$$F(W, t) = \frac{\langle W(t + \Delta t) - W(t) \rangle_W}{\Delta t}. \quad (16)$$

Here, $\langle \ldots \rangle_W$ denotes the conditional average that $W(t) = W$, which is applied in order to determine the functional dependence of the transport coefficients on the energy W (see, e.g., Ragwitz & Kantz 2001). In practice, the energies of the particles at time t are divided into bins of finite size and the

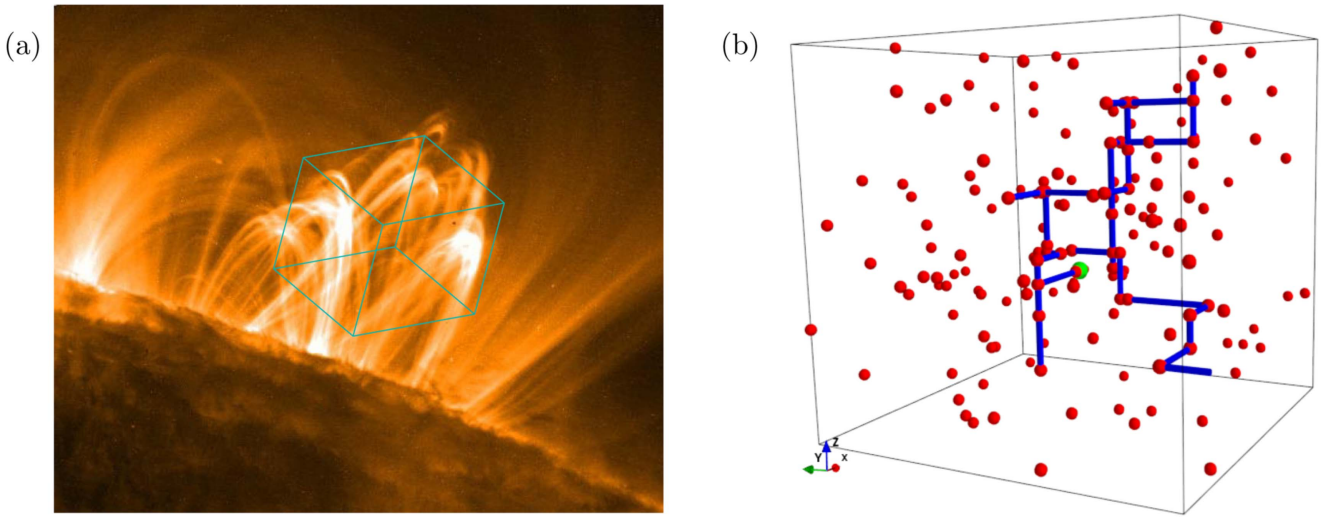

Figure 1. (a) Complex magnetic topology inside an active region, if it is disturbed by a magnetic perturbation, forms Alfvénic Scatters, which are one of the basic processes for coronal heating and particle acceleration during explosive energy release. (b) Trajectory of a typical particle (blue tube) inside a grid with linear dimension $L = 10^{10}$ cm. Active points are marked by spheres in red. The particle starts at a random grid point (green sphere) moves along a straight path on the grid until it meets an active point and then it moves into a new random direction, and so on, until it exits the simulation box.

transport coefficients are determined for each of the subsets of particles in the bins. Δt must be a small time interval, which should just be large enough so that most particles show measurable changes of the energy over the time interval Δt (theoretically the limit $\Delta t \to 0$ would apply).

3. Alfvénic Scatterers

3.1. Initial Setup

We construct a 3D grid ($N \times N \times N$) with linear size L, with grid size $\ell = L/(N-1)$. Each grid point is set as either *active* or *inactive*, i.e., a scatterer or not. Only a small fraction $R = N_{\rm sc}/N^3$ of the grid points are active (5%–15%). We can define the density of the scatterers as $n_{\rm sc} = R \times N^3/L^3$ and the mean free path of the particles between scatterers can be determined as $\lambda_{\rm sc} = \ell/R$. When a particle (an electron or an ion) encounters an active grid point it renews its energy state depending on the physical characteristic of the scatterer. It then moves in a random direction with its renewed velocity v until it meets another active point or exits the grid. The minimum distance between two scatterers is the grid size (ℓ). The time between two consecutive scatterings is $\Delta t = s/v$, where s is the distance the particle travels, which is an integer multiple of the minimum distance ℓ.

At time $t = 0$, all particles are located at random positions on the grid. The injected distribution $n(W, t = 0)$ is a Maxwellian with temperature T. The initial direction of motion of every particle is selected randomly.

3.2. Open Boundary Conditions

Here we are using the standard SFE process, as discussed in the previous section. The parameters used in this paper are related to the plasma parameters in the low solar corona. We choose the strength of the magnetic field to be $B = 100$ G, the density of the plasma $n_0 = 10^9\,{\rm cm}^{-3}$, the ambient temperature around 100 eV, and the length L of the simulation box is 10^{10} cm. The Alfvén speed is $V_A \approx 7 \cdot 10^8\,{\rm cm\,s}^{-1}$, so V_A is comparable with the thermal speed of the electrons. Each scattering changes the energy of a particle according to Equation (1). As the lattice constrains the motion, the term $\boldsymbol{V} \cdot \boldsymbol{v}$ can randomly assume only three possible values: -1 for head on scatterings, 1 for overtaking scatterings, and 0 for perpendicular scatterings. The typical energy increment is on the order of $(\Delta W/W) \approx (V_A/c)^2 \sim 10^{-4}$. We consider the grid to be open so particles can escape from the acceleration region when they reach any boundary of the grid at $t = t_{\rm esc}$, which of course is different for each escaping particle. We assume in this setup that only $R = 10\%$ of the $N^3 = 601^3$ grid points are active.

The ASs are formed through the propagation of large magnetic disturbances inside a complex magnetic topology (see Figure 1(a)). A typical trajectory of a particle inside the simulation box is displayed in Figure 1(b), the particles move along the grid on straight lines until they encounter a scatterer, which affects their energy and direction of motion (see Equation (1)). The motion of the particles is typical for a stochastic system with random-walk-like gain and loss of energy before exiting the simulation box. The mean free path is calculated as $\lambda_{\rm sc} = \ell/R \approx 1.7 \cdot 10^8$ cm, which coincides with the value estimated numerically by tracing particles inside the simulation box.

The temporal evolution of the mean kinetic energy of the electrons that remain inside the simulation box, by using the parameters stated above, is presented in Figure 2(a), along with the kinetic energy evolution of some typical energetic electrons. The energy increases exponentially (after a initial period of a few seconds), as expected from the analysis performed initially by Fermi (see Equation (4)). Using the analytical expression derived by Fermi, Equation (2), we estimate $t_{\rm acc_{th}} = (3\lambda_{\rm sc}c)/(4V_A^2) \approx 8$ s. We can also estimate the acceleration time from our simulation by making an exponential fit to the asymptotic exponential form of the mean kinetic energy, as predicted by Equation (4), which yields an acceleration time of $t_{\rm acc_{num}} \approx 9$ s, a value close to the analytical estimate. In Figure 2(b), we show the mean energy of the particles that remain inside the box during the transient phase (the first 10 s), which increases as $\langle W(t) \rangle \sim t^{1.6}$, thus following a scaling close to the prediction of the hard sphere approximation (see Equation (11)), and being in correspondence with

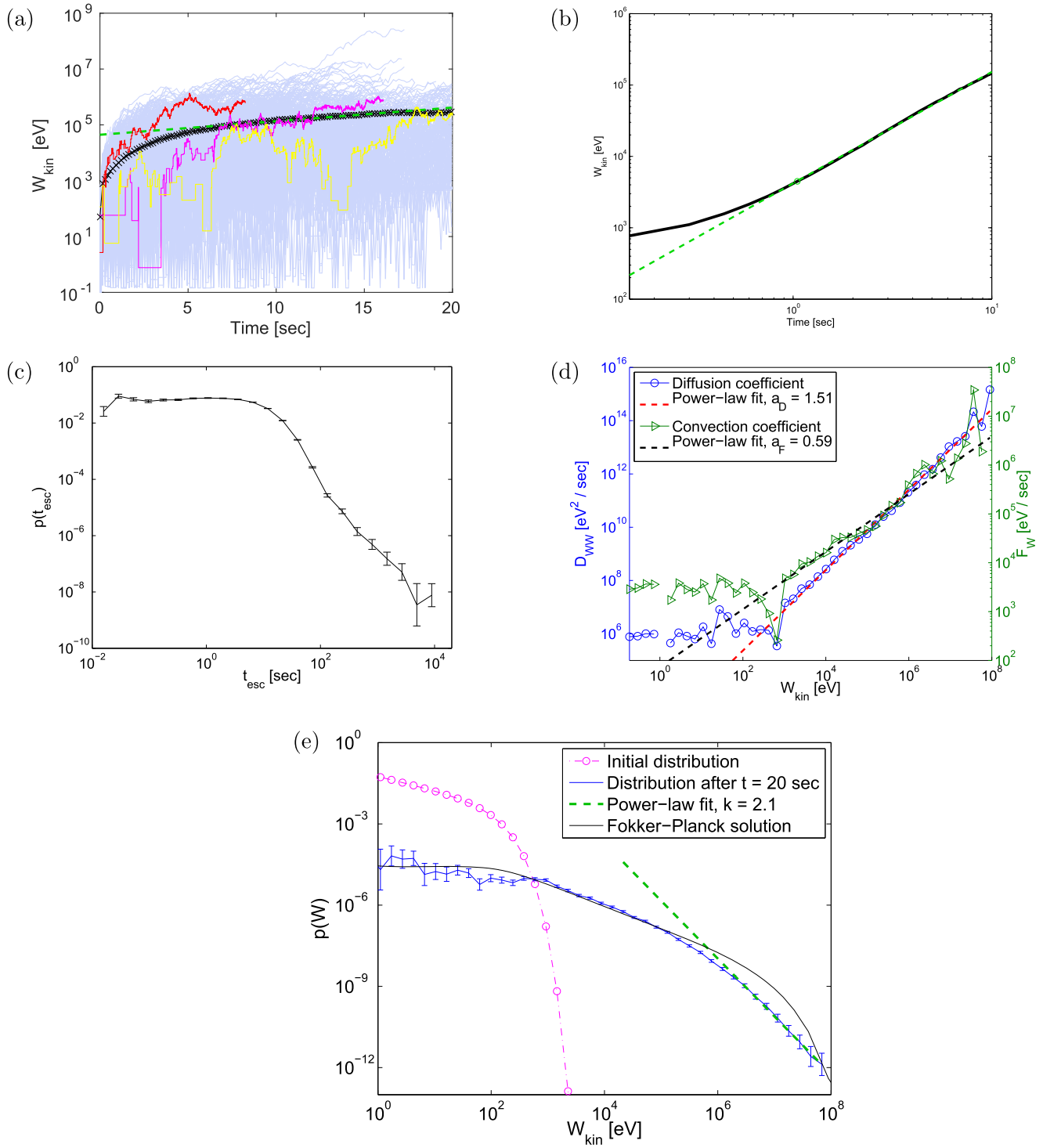

Figure 2. (a) Kinetic energy of the electrons remaining inside the box as a function of time (blue), their mean energy (black) with an exponential fit (green), and the kinetic energy of three typical electrons. (b) Transient phase of the temporal evolution of the mean kinetic energy of all the particles (black) together with a power-law fit ($\sim t^{1.6}$, green). (c) Distribution of the escape time of the electrons. (d) Energy diffusion and convection coefficients as functions of the kinetic energy at time $t = 20$ s. (e) Energy distribution at $t = 0$ and $t = 20$ s (stabilized) for the electrons remaining inside the box and the corresponding solution of the Fokker–Planck equation.

the functional form of the convection coefficient as estimated below. Figure 2(c) presents the escape-time distribution for all electrons (i.e., the time they have reached any boundary); it starts as a uniform distribution at low values and turns over to a power-law distribution at large values. Here we use the median value (≈8 s) as an estimate for a characteristic escape time from the system, $t_{\rm esc}$.

The energy distribution function of the electrons remaining inside the box is a synthesis of a hot plasma with a mean temperature ≈100 keV and a power-law tail (see Figure 2(e)). The power-law index is $k \approx 2.1$ after about 20 s and the power-law tail is extended up to 100 MeV. If we use the values for $t_{\rm acc}$ and $t_{\rm esc}$ estimated above, the simple expression in Equation (8) gives an estimate of the slope of the tail as

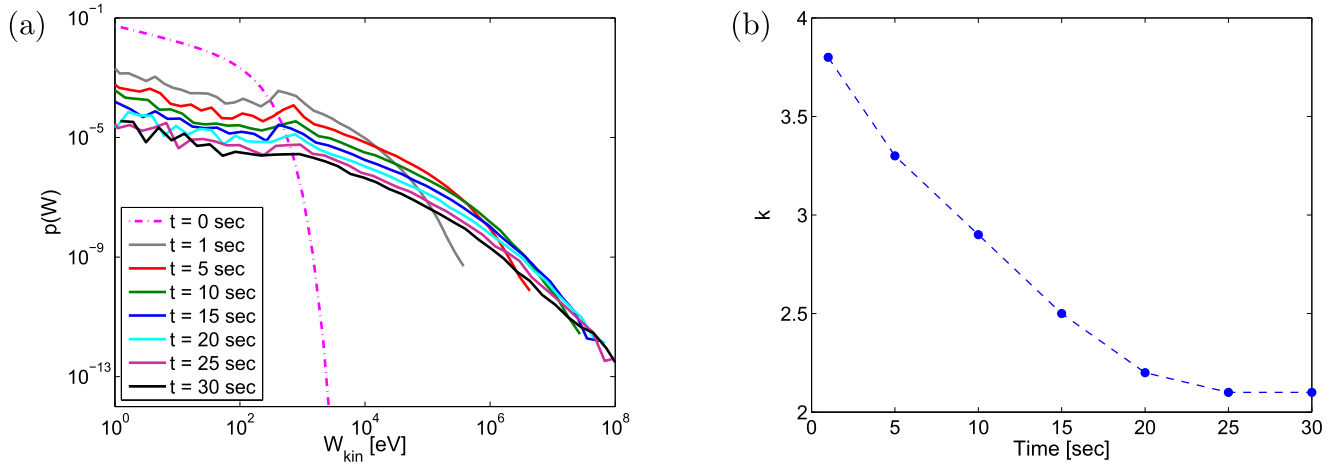

Figure 3. (a) Energy distribution at various times for the electrons that remain inside the box. (b) Power-law index of the tail of the energy distribution at various times.

$k = 1 + t_{\rm acc}/t_{\rm esc} \approx 1 + 9/8 \approx 2.1$, which is identical to the numerical result derived from the simulation. Using the hard sphere model (see Equation (13)), we obtain a very similar result for the power-law index ($k \approx 1.9$).

In Figure 2(d), the diffusion and convection coefficients at $t = 20$ s, as functions of the energy, are presented. The estimate of the coefficients is based on Equations (15) and (16), with Δt small, whereto we monitor the energy of the electrons at a number of regularly spaced monitoring times $t_k^{(M)}$, $k = 0, 1, \ldots, K$, with K typically chosen as 200, and we use $t = t_{K-1}^{(M)}$, $\Delta t = t_K^{(M)} - t_{K-1}^{(M)}$ in the estimates. Also, in order to account for the conditional averaging in Equations (15) and (16), we divide the energies $W(t_{K-1}^{(M)})_i$ of the particles into a number of logarithmically equi-spaced bins and perform the requested averages separately for the particles in each bin. As Figure 2(d) shows, both transport coefficients exhibit a power-law shape for energies above 1 keV, $D(W) = 223.57\ W^{1.51}$, and $F(W) = 73.47\ W^{0.59}$. These results agree quite well with the estimates reported above (Equations (9) and (10)) from the hard sphere model of Parker & Tidman (1958) and Ramaty (1979).

In order to verify the estimates of the transport coefficients, we insert them into the FP equation (Equation (5)) and solve the FP equation numerically in the form

$$\frac{\partial n}{\partial t} + \frac{\partial}{\partial W}\left[Fn - \frac{\partial (Dn)}{\partial W}\right] = -\frac{n}{t_{\rm esc}}, \qquad (17)$$

including the escape term $-n/t_{\rm esc}$, with $t_{\rm esc} = 8$ s as the median value from Figure 2(c). The transport coefficients are inserted in the form of the fit above 1 keV and set to constant below 1 keV such that they are continuous at the transition. For the integration of the FP equation on the semi-infinite energy interval $[0, \infty)$, we use the pseudospectral method, based on the expansion in terms of rational Chebyshev polynomials in energy space, combined with the implicit backward Euler method for the time-stepping (see, e.g., Boyd 2000). The resulting energy distribution at final time is also shown in Figure 2(e), and it turns out to coincide very well with the distribution from the electron simulation in the intermediate energy range that corresponds to the heating of the population, though the power-law tail cannot be reproduced in shape by the FP solution.

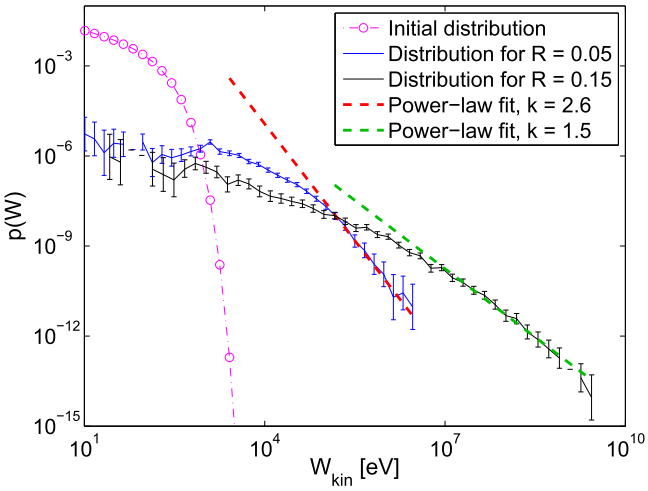

Figure 4. Stabilized energy distribution for electrons remaining inside the box at $t = 0$ and $t = 25$ s for $R = 0.05$ ($\lambda_{\rm sc} = 3.3 \cdot 10^8$ cm) (blue) and $R = 0.15$ ($\lambda_{\rm sc} = 1.1 \cdot 10^8$ cm) (black).

The heating and the power-law tail in the energy distribution function are formed almost from the start of our simulation and reach their asymptotic shape on a timescale comparable with the acceleration time (see Figure 3(a)). In the beginning, the power-law index is ≈5 and it gradually decreases until it reaches an asymptotic value 2.1 in about 20 s (almost twice the acceleration time), as shown in Figure 3(b).

In the case of parameters that we considered, the escape time is locked to the acceleration time ($t_{\rm acc} \approx t_{\rm esc}$), therefore the density of the scatterers, which controls the mean free path, is the most important parameter for our system. A parametric study of the evolution of the energy distribution of the particles, as we vary the density of the scatterers $0.05 < R < 0.15$ (i.e., $1.1 \cdot 10^8 < \lambda_{\rm sc} < 3.3 \cdot 10^8$), keeping the characteristic length of the acceleration volume constant, was made and we find that the escape time varies between $5\ {\rm s} < t_{\rm esc} < 8\ {\rm s}$, while the acceleration time decreases from ≈8 s to ≈4 s. The power-law tail index also decreases and it remains close to $3 \gtrapprox k \gtrapprox 1.5$. In Figure 4, we show stabilized distribution functions for $R = 0.05$ and $R = 1.5$. The time when the k-index stabilizes varies between 20 and 25 s.

We have performed an extensive analysis of the role of the free parameters (R, as just described, and also N and L) in our

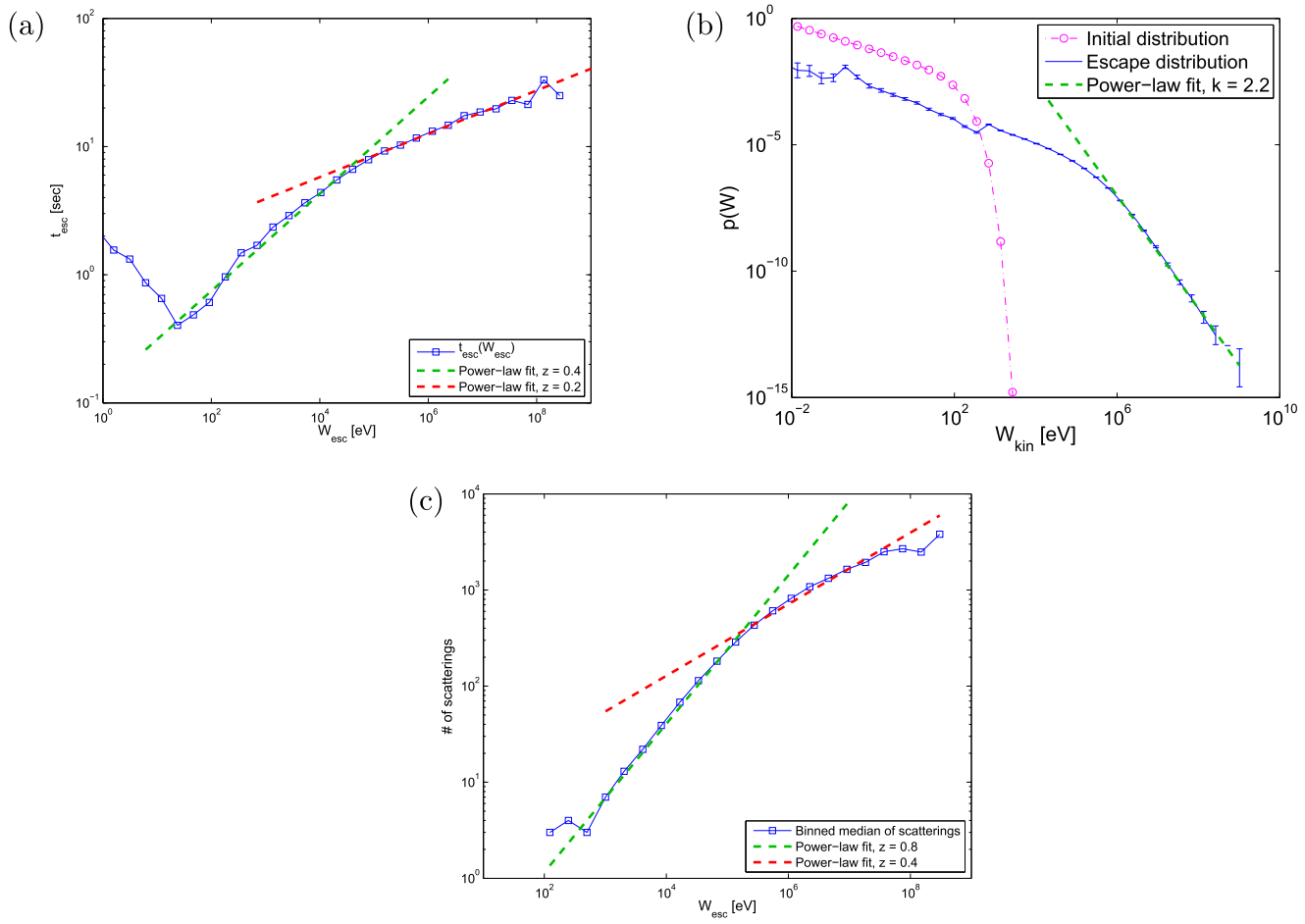

Figure 5. (a) Escape time as a function of the escape energy of the electrons. (b) Energy distribution of the electrons that have escaped from the box. (c) Mean number of scatterings per particle as a function of the escape energy.

results and we conclude that, if in our setup for the physical system under investigation we keep the mean free path of the particles (λ_{sc}) constant, the main results presented above remain the same.

Depending on the initial energy and the energization in the scattering events, each of the escaping electrons leaves the acceleration volume with a different energy and at a different time. We have already shown the distribution of the escape times t_{esc} in Figure 2(c). In Figure 5(b), we present the energy distribution of the escaped electrons, $p(W_{esc})$, which has a shape very similar to the one of the energy distribution shown in Figure 2(e) of the particles that remain inside the simulation box until saturation, and it exhibits a thermal distribution for the low-energy particles ($W < 100$ KeV) and a power-law tail for the relativistic particles with energies $W > 1$ MeV. In Figure 5(a), we show the mean escape time as a function of the energy with which the particles escape from the turbulent volume, and it follows a power-law distribution, $t_{esc} \propto W_{esc}^{z}$. We observe two distinct regions: for the non-relativistic energies, 10–10^5 eV, the exponent is $z = 0.4$, while for the relativistic particles, 10^5–10^9 eV, the exponent drops to $z = 0.2$. The relation of t_{esc} with the escape energy of the electrons can be understood by the fact that energization should closely be connected with the trapping of the particles by the ASs. The correlation of the trapping of the electrons with their final energy can be demonstrated when considering the mean number of scatterings the escaping particles suffer before they escape from the simulation box as a function of their energy, as shown in Figure 5(c), from which it is clear that the energization depends strongly on the trapping of the particles inside the turbulent volume, and thus, the longer they stay inside, the more they are accelerated. This result is clearly very different from the t_{esc} used in the literature on stochastic weak turbulence acceleration ($t_{esc} \approx L/v$; see Miller et al. 1990; Petrosian 2012), but it seems to agree qualitatively with the observational results obtained by Petrosian & Chen (2010), although their estimate is based on a very simple magnetic topology, e.g., a simple magnetic loop. The trapping of the energetic particles inside the turbulent volume, where acceleration and heating takes place, seems to solve another well documented observation, the relatively long life of hard X-ray sources following CMEs in the high corona (Krucker et al. 2007). As we have shown, the strong trapping of the electrons for tens of seconds inside the ASs can explain this observation.

Our results so far refer only to electrons. The ions in the asymptotic state do not have significant differences from the evolution of the electrons, other than the timescale needed to reach this state. The energy distribution exhibits the same characteristics (heating and acceleration) and it saturates after 27 s; in Figure 6(c), we show the saturated distribution of the ions remaining inside the domain at $t = 30$ s, it extends up to tens of GeV. The median escape time is ≈26 s and the acceleration time calculated from the analytical expression in Equation (2) remains unchanged; the numerically estimated

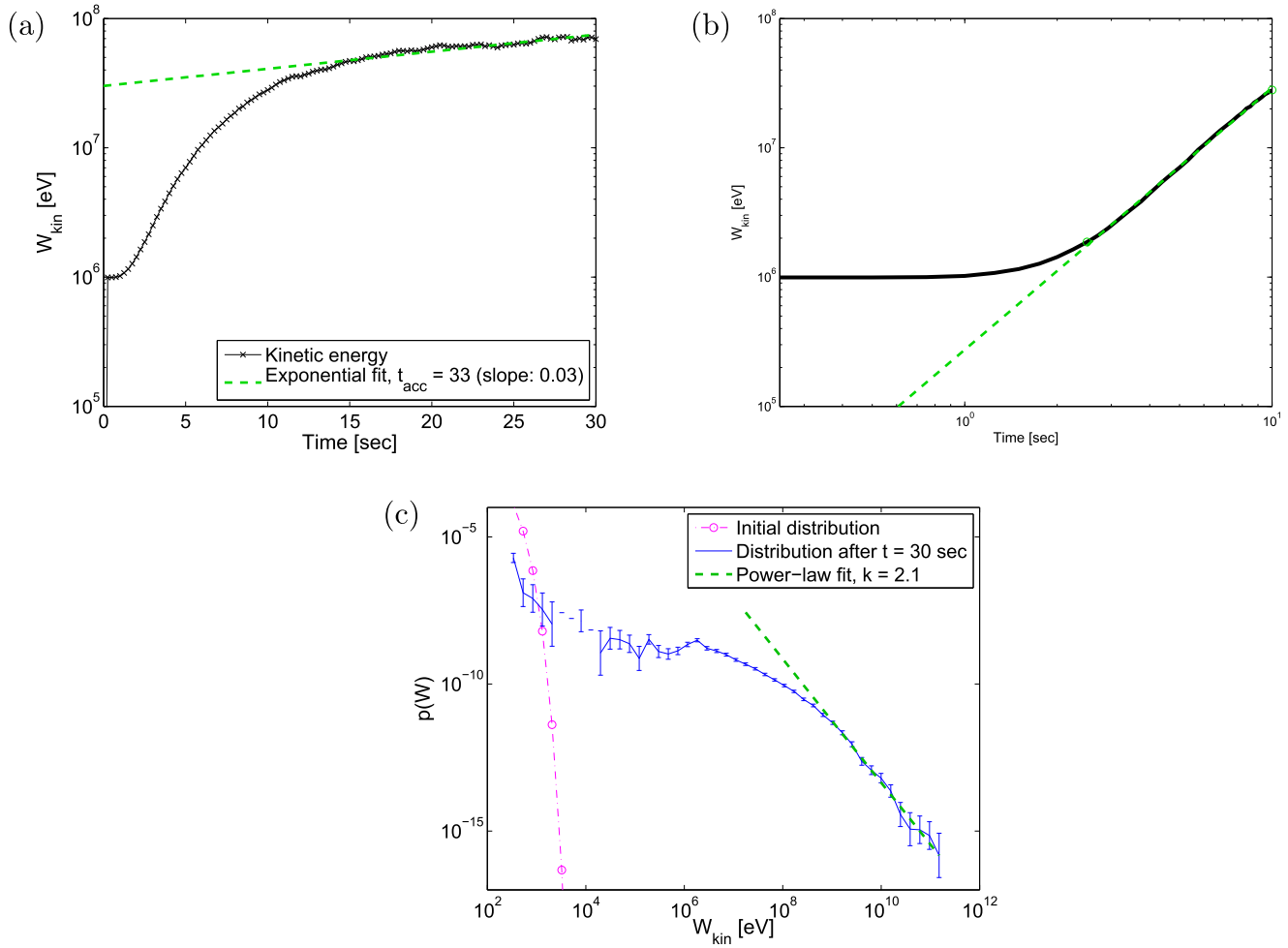

Figure 6. (a) Mean kinetic energy of the ions remaining inside the box, as a function of time (black) with an exponential fit (green). (b) Temporal evolution of the mean kinetic energy of all the ions in the transient phase (the first seconds, black), along with a power-law fit ($\sim t^2$, green). (c) Energy distribution at $t = 0$ and $t = 30$ s (stabilized) for the ions remaining inside the box.

value, through Equation (4), is $t_{\mathrm{acc}_{\mathrm{num}}} \approx 33$ s (see Figure 6(a); as for the electrons, the mean energy evolves as a power law in the the transient phase, see Figure 6(b)). Applying these two values in Equation (8) leads to $k \approx 2.1$, which agrees with the measured slope of the power-law tail in the energy distribution.

We can then conclude that SFE can heat and accelerate both ions and electrons in the solar corona to a level as it is observed.

3.2.1. The Role of Collisions in the Evolution of the Energy Distribution

We apply a modification of the simplified model of Lenard & Bernstein (1958) for the Coulomb collisions of charged particles with a background plasma population of temperature T (which coincides with the colliding particles' initial temperature in our approach),

$$\frac{ds}{dt} = v,$$
$$\frac{dv}{dt} = -\nu_v v + \sqrt{2\nu_v k_B T/m}\ N_t, \tag{18}$$

where k_B is the Boltzmann constant and N_t an independent and identically distributed Gaussian random variable with mean value zero and variance the integration time-step Δt. Within this model, a particle travels a distance s between two consecutive scatterers (which is an integer multiple of l) for a time interval τ, with non-constant velocity due to collisions with the background plasma. Following Gillespie (1996), we directly use the analytical solution to Equation (18),

$$v(t+\tau) = v(t)\mu + \sigma_v N_1, \tag{19}$$

with $\mu = e^{-\nu_v \tau}$, $\sigma_v^2 = \frac{k_B T}{m}(1-\mu^2)$, and N_1 a Gaussian random variable with mean 0 and standard deviation 1, which allows us to use arbitrarily large timesteps and is thus computationally favorable. The use of the analytical solution allows to make the Lenard & Bernstein (1958) collision model more realistic than it is in its standard form, namely by making the collision frequency velocity dependent, $\nu_v \propto 1/v^3$, as appropriate for a fully ionized plasma (see, e.g., Karney 1986), with v the instantaneous velocity of a particle before each of the collisionally affected travel events in between subsequent scatterings. We also note that v here is the non-relativistic speed that is bounded by the speed of light, the characteristic scaling thus breaks down for very energetic particles.

In Figure 7, we present the energy distribution of electrons with and without collisions at two instances, one before ($t = 10$ s) and one after its stabilization ($t = 25$ s). Even

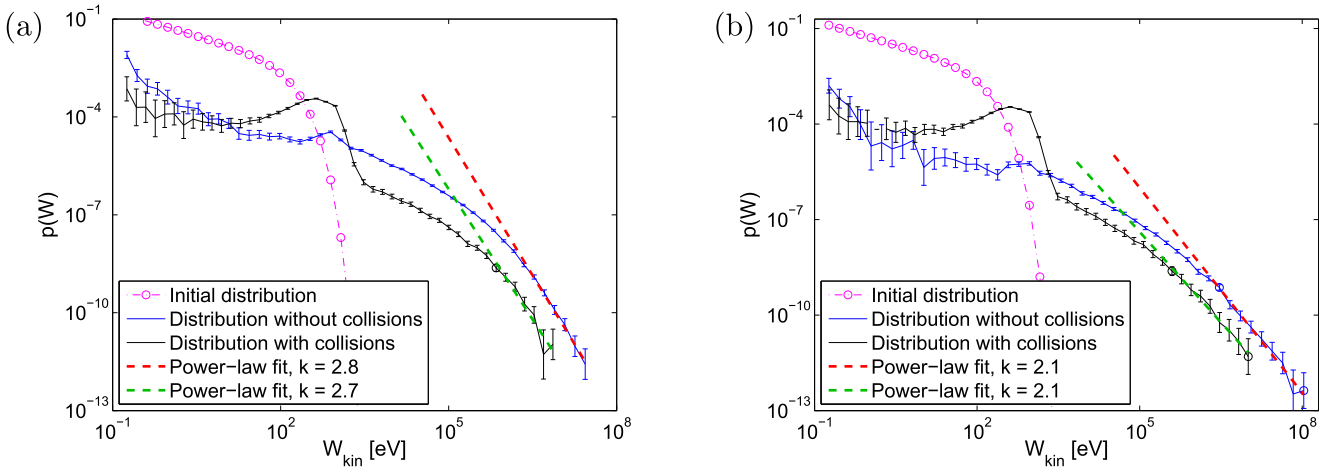

Figure 7. (a) Energy distribution for electrons remaining inside the simulation box (a) at $t = 0$ (magenta) and at $t = 10$ s with collisions (black) and without (blue), and (b) at $t = 25$ s, after the stabilization.

though the mean free path for the collisions is almost 20 times smaller than the mean free path for the scattering ($\lambda_{\rm coll} = 7.67 \cdot 10^6$ cm), for the characteristic timescale of the interaction we consider (e.g., the acceleration time), the distribution separates into the low to intermediate energy part (300 eV–3 keV), where the collisions dominate and the evolution of the energy distribution approaches a Maxwellian distribution, and the higher energy part, where the energization dominates and the electrons are accelerated, forming a power-law tail with index similar to the one of the collisionless case, though slightly reduced in extent.

3.3. Periodic Boundary Conditions

Keeping the setup outlined above, we now impose periodic boundary conditions on the grid, i.e., when an electron reaches any boundary of the grid, it re-enters from the corresponding grid point at the opposite boundary. We only reduce R down to 0.05, since, due to the trapping in the acceleration volume, the energization is much more efficient and the electrons reach very quickly relativistic velocities. The electrons are monitored over a time interval sufficiently large for the power-law index to stabilize, e.g., for 35 s (see Figure 8).

The initial and the final distribution of the energy of the electrons after 35 s are shown in Figure 8(e). By this time the distribution can be considered "asymptotic," meaning that the power-law tail index has decreased to $k \approx 3$ and it stabilizes at that value, the system thus has the same characteristics as in the open-boundary case, see Figure 2(e).

The temporal evolution of the mean kinetic energy of the electrons and ions is similar to the open box case analyzed above (see Figure 8(a)). The energy of the electrons increases exponentially after a short transient period (during which the mean energy follows a power-law evolution over time, $\langle W \rangle \sim t^{2.1}$ (see Figure 8(b)), as it is predicted for the non-relativistic particles by the hard sphere approximation), giving a numerical estimate of the acceleration time of $t_{\rm acc_{num}} \approx 8$ s, which is equal to $t_{\rm acc_{th}}$.

In Figure 8(d) the diffusion and convection coefficients at $t = 35$ s, as functions of the energy, are presented. They both exhibit a power-law shape for energies above 1 keV, $D(W) = 37.98\ W^{1.58}$, and $F(W) = 38.57\ W^{0.59}$. The indices are thus very close to the ones of the power laws in the open-boundary case. We again use the estimated transport coefficients in the FP equation (Equation (17), for $t_{\rm esc} = \infty$), solving it numerically as before, and the resulting energy distribution at final time is shown in Figure 8(e), which shows that we again have very good coincidence in the intermediate to high-energy range, and some deviations in the highest energy range.

As in the open boundaries case discussed above, $\lambda_{\rm sc}$ is the key parameter that affects the evolution of the system. Keeping the characteristic length of the acceleration volume constant and varying the density of the scatterers in the range $0.05 < R < 0.20$ (i.e., $3.3 \cdot 10^8$ cm $< \lambda_{\rm sc} < 8.3 \cdot 10^7$ cm), the acceleration time decreases from $\approx$8 s to $\approx$2 s with increasing R, and the power-law tail index k decreases from $k \approx 3$ to $k \approx 2$. The saturation time for the k-index lies within 25 and 35 s, so the quantitative behavior of the system depends indeed strongly on the mean free path of the interaction of the particles with the scatterers, $\lambda_{\rm sc}$.

4. Discussion

Stochastic acceleration of electrons and ions by weak turbulence during solar flares has been discussed extensively in the astrophysical literature (see the reviews by Miller et al. 1997; Petrosian 2012). Several questions on the stochastic acceleration by weak turbulence still remain open. Let us note a few here. (a) The term "turbulence" in these studies means "a spectrum of MHD waves with low amplitude ($\delta B/B \ll 1$)" and the excited waves cover a specific range of wavenumbers so that the resonant or transient acceleration of the particles by the waves can reach very high energies. The spectrum of the waves is assumed to be a power law with specific slope. The excitation or the formation by nonlinear wave–wave interaction of the specific spectrum, with the characteristics outlined above, through an explosive energy release in a complex magnetic topology remains an open question. (b) The transport coefficients are estimated with the use of the quasilinear approximation, which is valid only for weak turbulence. (c) The escape time has never been quantitatively estimated and it is used as a free parameter, calculated from the simple relation $t_{\rm esc} \approx L/v$, where L is the characteristic size of the acceleration volume and v the velocity of the energized particles. Therefore, returning back to the three questions posed in the introduction, we conclude that: (1) the constraints posed for the validity of the theory of SAT are very severe, and its relation with the

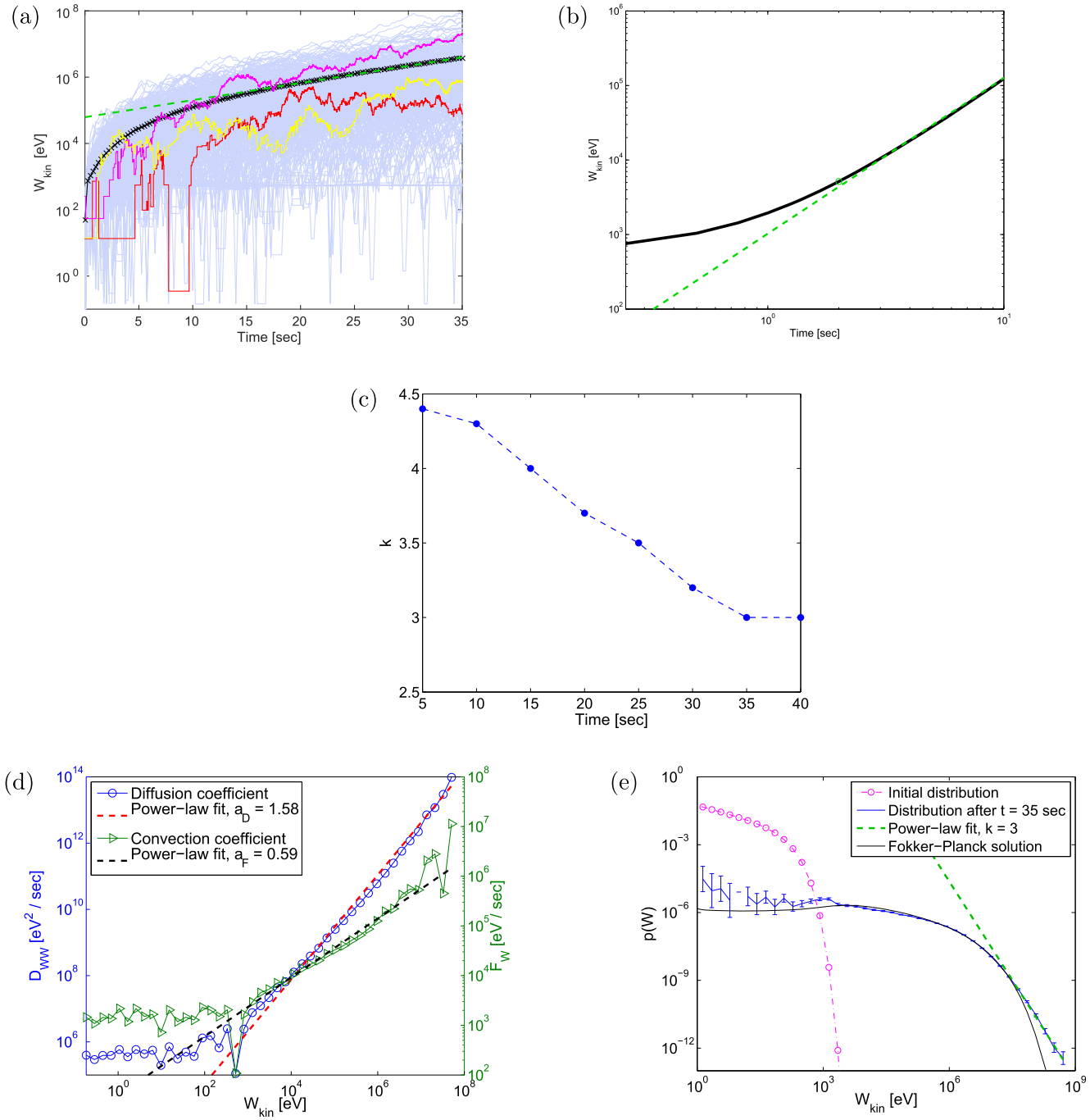

Figure 8. (a) Kinetic energy of the electrons as a function of time (blue), their mean energy (black) with an exponential fit (green), and the kinetic energy of three typical electrons. (b) Temporal evolution of the mean kinetic energy of all the electrons in the transient phase (the first seconds, black), together with a power-law fit ($\sim t^{2.1}$, green line). (c) Power-law index of the tail of the distribution at various times up to its stabilization. (d) Energy diffusion and convection coefficients as functions of the kinetic energy. (e) Energy distribution at $t = 0$ and $t = 35$ s for the electrons remaining inside the box, and the corresponding solution of the Fokker–Planck equation.

original concept proposed by Fermi, the stochastic Fermi Energization, is questionable. (2) We have shown that the escape time, which follows closely the acceleration time $t_{\rm acc}$ in the asymptotic state of the interaction of particles with AS, is an increasing function of the particle energy. This result is in agreement with recent observations (Petrosian & Chen 2010), although with some caution, due to the relatively simple topology assumed by the authors in their analysis, which is contrary to the assumptions made in this paper. (3) Based on the solution of the Fokker–Planck equation and our numerical results, we have shown that when the transport coefficients are estimated properly the trapped particles sustain heating and acceleration of the plasma in a similar fashion with the non-trapped particles.

We have revisited in this paper the initial proposal put forward by Fermi (1949) and re-introduced the concept of "magnetic clouds" as "Alfvénic Scatterers", based on strong local magnetic fluctuations ($\delta B/B \approx 1$), formed at a small number of random places inside a complex magnetic topology and traveling with the Alfvén speed. Summing up the total

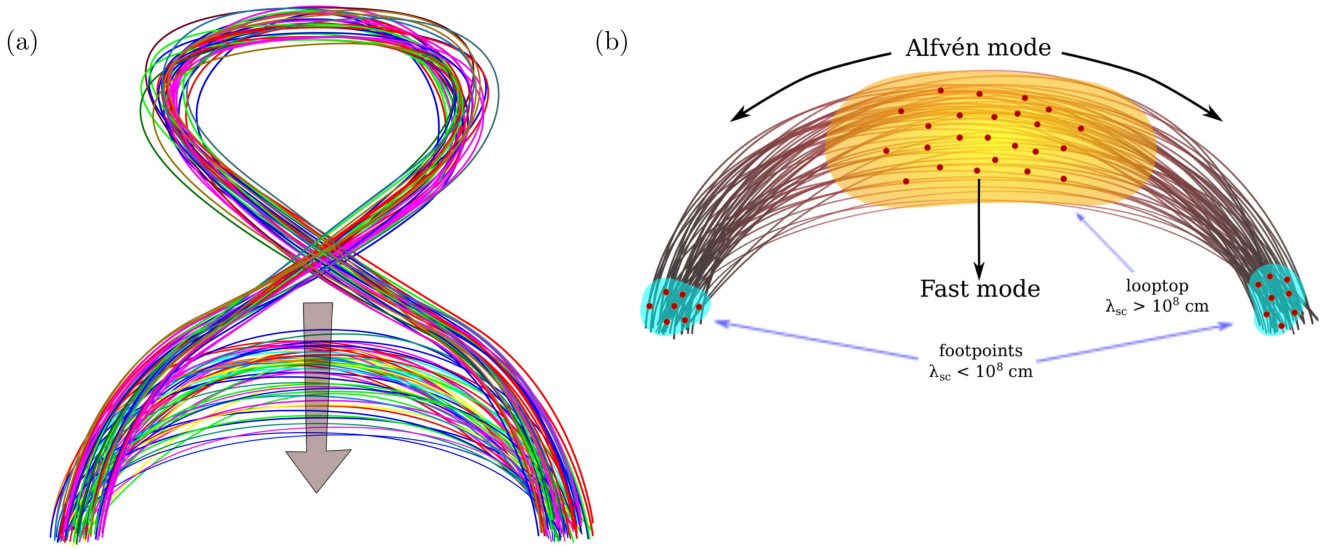

Figure 9. (a) Loss of stability of a large-scale magnetic structure will initiate unstable current sheets and launch a large-scale disturbance, which will drive AS in the 3D topology associated with the unstable structure. (b) In the collapsing structures, ASs (marked here with red dots) are formed inside the complex magnetic topology at the top and the footpoints, with very similar λ_{sc}. The plasma at the top is intensely heated, particles are accelerated, and it is trapped for relatively long times. The footpoints are simultaneously energized through the AS formed by the MHD disturbance.

energy carried by the random fluctuations ($U_{\delta B}$) and dividing by the energy carried by the ambient magnetic field U_B, the weak turbulent approximation ($U_{\delta B}/U_B \ll 1$) is still valid, but here the energy is localized and carried by the moving coherent structures. As we have shown in this paper, the interaction of ions and electrons with the AS is a relatively simple and, at the same time, a very efficient mechanism for their heating and acceleration. Several aspects from our analysis can now be put in context in the energization of plasmas in the solar atmosphere during explosive events. The most important finding from our analysis is that the fast (on a timescale of about $t_{acc} \approx 10$–20 s) heating and acceleration of the plasma particles depends on one parameter only: the mean free path of the particles interacting with the localized magnetic fluctuations (λ_{sc}). The energy distribution of the electrons reaches an asymptotic form with temperature around 10 keV and a power-law tail with index $k \approx 2$ for $\lambda_{sc} \approx 10^8$ cm.

Based on the above findings, we propose a very simple four-step scenario for the heating of the plasma and the acceleration of particles during the explosive phenomena on the Sun, which in our opinion solves a number of open questions that have been posed by current observations.

1. Step 1: (*Start of the magnetic instability and formation of UCS*) The loss of equilibrium of large-scale structures (based, as we outlined in the introduction, on magnetic flux emergences from the convection zone, loss of stability of loops, and the violent shuffling of magnetic field lines at the footpoints of closed loops) will initiate a major reconstruction of the large-scale magnetic topology and will cause the formation of UCS of all scales (see Figure 9(a), and Gordovskyy et al. 2014).
2. Step 2: (Large-scale*magnetic reconstruction and launch of a large-scale MHD disturbance*) The formation of complex magnetic topologies based on the violent reconstruction of the magnetic field during the launch of a magnetic disturbance on all scales due to the formation of UCS inside the unstable magnetic configuration (see Figure 9(a)). Steps 1 and 2 are following the scenario proposed by Fletcher & Hudson (2008) and are implemented numerically by Gordovskyy et al. (2014), considering the deposition of energy in the low corona and upper chromosphere by large-scale MHD disturbances during the collapse of a complex magnetic topology.
3. Step 3: (*Formation of AS and UCS at random places inside the unstable magnetic topology*) The formation of AS and UCS through the propagation of the large-scale disturbances in the complex magnetic structures (see Figure 9(b) and Figure 5 in Gordovskyy et al. 2014).
4. Step 4: (*loop top, footpoints, and chromospheric heating*) The AS and UCS formed in the closed magnetic topology (Figure 9(b)) have $\lambda_{sc} > 10^8$ cm at the loop top, where particles will be trapped, heated, and accelerated for relatively long times (see Krucker et al. 2007, 2008). More details for this process are presented in Section 3.3 about the AS. The interaction of the plasma with the UCS has been discussed briefly by Vlahos et al. (2016). The MHD disturbance forming the AS will reach the two footpoints simultaneously and since λ_{sc} is approximately the same at the footpoints and possibly smaller than at the loop top, the heating and the acceleration of particles will locally be more intense (see Section 3.2 and Figure 9(a)) and will compete favorably with the local Coulomb collisions, as it already does at the loop-tops (see Section 3.2.1 and Figure 9(b)). It would be interesting to analyze the propagation of the magnetic disturbance into the chromosphere and to study if the local heating can be efficient when λ_{sc} starts becoming comparable with the collisional mean free path (see Section 3.2.1).

The proposed scenario provides a way for the initial suggestions made by Fermi to energize the solar plasma during explosive events without the need of a large number of particles to be transported from the coronal part of the unstable structure to the low corona and the upper chromosphere.

5. Summary

We developed a 3D lattice model where a small fraction of grid points acts as "scatterers," in accordance with the initial suggestion of Fermi (1949) and the work of Parker & Tidman (1958) and Ramaty (1979). In our work, the emphasis is put on the coherent local fluctuations inside a complex magnetic topology, which are moving with the Alfvén speed, and which we here refer to as "AS," and the initial Fermi approach as SFE.

The main results from our study are as follows.

1. The SFE can reproduce the well-known energy distribution of astrophysical plasmas, where heating of the bulk and acceleration of the energetic particles co-exist.
2. The density of the scatterers (or equivalently, the mean free path λ_{sc} of the interaction of the particles with the AS) controls the heating and the evolution of the energetic particles.
3. The energy distribution reaches an asymptotic state on a timescale comparable to the acceleration time t_{acc}. Similar results have been reported on the interaction of ions with a spectrum of Alfvén waves or electrons with a spectrum of whistler waves (see Miller et al. 1990). When the energy distribution reaches the asymptotic state, the mean escape time of the particles t_{esc} is comparable with t_{acc} if $\lambda_{sc} \approx 10^8$ cm.
4. The index of the power law of the particles in the energetic tail in the asymptotic state seems to agree very well with the simple formula derived by Fermi, $k = 1 + t_{acc}/t_{esc}$ and with the estimates of Parker & Tidman (1958) and Ramaty (1979) for $W \gg mc^2$.
5. The escape time has a power-law dependence on the energy of the particles, $t_{esc} \sim W^{0.3}$, which is different from the relation used in the analysis of the stochastic acceleration by waves and it agrees qualitatively with observations (see Krucker et al. 2007; Petrosian & Chen 2010). Yet, a more careful modeling is needed, both for the long trapping of the hard X-rays in the high corona (Krucker et al. 2007) and for the results reported by Petrosian & Chen (2010).
6. The transport coefficients are estimated from the dynamics of the particles interacting with the AS; the systematic acceleration coefficient has the form $F \sim W^{a_F}$ and the diffusion coefficient the form $D \sim W^{a_D}$, where $a_F = 0.59$ and $a_D = 1.51$, quite close to the values predicted in the hard sphere approximation of Parker & Tidman (1958) and Ramaty (1979). The solution of the FP equation conforms well with the energy distribution derived from our numerical simulation of the dynamic evolution of the particles, in the low and up to mildly relativistic energy regimes.
7. Collisions slow down the low-energy electrons and ions and do not influence the power-law index in the asymptotic state.
8. The trapped particles (periodic boundary conditions) are energized much more efficiently than the particles in the open system. For this reason we have used a longer mean free path and the system reaches the asymptotic state on a longer timescale and the energy distribution of the energetic particles has a softer power-law index. The overall characteristics of the energy distribution are similar to the results reported for the open box. The transport coefficients were again estimated from the trajectories of the particles, and the solution of the FP equation agrees with the energy distribution estimated from the simulation of the dynamic evolution of the particles.

In summary, the formation of large-scale local magnetic fluctuation ($\delta B/B \approx 1$) inside complex magnetic topologies during explosive phenomena forced us to reconsider the original SFE process. We note that the SFE process has only one free parameter, the mean free path λ_{sc}.

Many question remain open and will be discussed in future publications. For example, what will happen to the system analyzed here if the AS is replaced by UCS (see Vlahos et al. 2016)? What will happen to a beam of particles interacting with the AS and being re-accelerated as they propagate inside the complex magnetic topology? What will happen at a strong shock if the AS and UCS upstream and downstream of the shock surface are treated with the tools reported in this study?

We thank the anonymous referee for helpful comments and suggestions. The authors acknowledge support by European Union (European Social Fund—ESF) and Greek national funds through the Operational Program Education and Lifelong Learning of the National Strategic Reference Framework (NSRF)—Research Funding Program: Thales: Investing in knowledge society through the European Social Fund.

References

Achterberg, A. 1981, A&A, 97, 259
Amari, T., Aly, J.-J., Canou, A., & Mikic, Z. 2013, A&A, 553, A43
Archontis, V. 2008, JGRA, 113, A03S04
Boyd, J. P. 2000, Chebyshev and Fourier Spectral Methods (2nd ed., New York: Dover Publications)
Davis, L. 1956, PhRv, 101, 351
Fermi, E. 1949, PhRv, 75, 1169
Fletcher, L., Cargill, P. J., Antiochos, S. K., & Gudiksen, B. V. 2015, SSRv, 188, 211
Fletcher, L., & Hudson, H. S. 2008, ApJ, 675, 1645
Galsgaard, K., & Nordlund, Å. 1996, JGR, 101, 13445
Gerrard, C. L., & Hood, A. W. 2003, SoPh, 214, 151
Gillespie, D. T. 1996, PhRvE, 54, 2084
Gordovskyy, M., & Browning, P. K. 2011, ApJ, 729, 101
Gordovskyy, M., & Browning, P. K. 2012, SoPh, 277, 299
Gordovskyy, M., Browning, P. K., Kontar, E. P., & Bian, N. H. 2014, A&A, 561, 72
Greco, A., Perri, S., & Zimbardo, G. 2010, JGRA, 115, A02203
Hamilton, R. J., & Petrosian, V. 1992, ApJ, 398, 350
Karney, C. F. F. 1986, CoPhR, 4, 183
Krucker, S., Battaglia, M., Cargill, P. J., et al. 2008, A&ARv, 16, 155
Krucker, S., White, S. M., & Lin, R. P. , 2007, ApJL, 669, L49
Kulsrud, R. M., & Ferrari, A. 1971, Ap&SS, 12, 302
Leake, J. E., Linton, M. G., & Antiochos, S. K. 2014, ApJ, 787, 46
Lenard, A., & Bernstein, I. B. 1958, PhRv, 112, 1456
Longair, M. S. 2011, High Energy Astrophysics (Cambridge: Cambridge Univ. Press)
Miller, J. A., Cargill, P. J., Emslie, A. G., et al. 1997, JGR, 102, 14631
Miller, J. A., Guessoum, N., & Ramaty, R. 1990, ApJ, 361, 701
Parker, E. N. 1983, ApJ, 264, 635
Parker, E. N. 1994, Spontaneous Current Sheets in Magnetic Fields: with Applications to Stellar X-rays (Vol. 1; New York: Oxford Univ. Press), 1
Parker, E. N., & Tidman, D. A. 1958, PhRv, 111, 1206
Petrosian, V. 2012, SSRv, 173, 535
Petrosian, V., & Chen, Q. 2010, ApJL, 712, L131
Ragwitz, M., & Kantz, H. 2001, PhRvL, 87, 254501
Ramaty, R. 1979, in AIP Conf. Proc. 56, Particle Acceleration Mechanisms in Astrophysics, ed. J. Arons, C. Max, & C. McKee (New York: AIP), 135
Schlickeiser, R. 1989, ApJ, 336, 243
Schmieder, B., Archontis, V., & Pariat, E. 2014, SSRv, 186, 227
Similon, P. L., & Sudan, R. N. 1989, ApJ, 336, 442
Török, T., Leake, J. E., Titov, V. S., et al. 2014, ApJL, 782, L10
Tverskoi, B. A. 1967, SvA, 10, 1031
Vlahos, L., Pisokas, T., Isliker, H., Tsiolis, V., & Anastasiadis, A. 2016, ApJL, 827, L3